Journal of Photochemistry & Photobiology, B: Biology 180 (2018) 39–50

Contents lists available at ScienceDirect

Journal of Photochemistry & Photobiology, B: Biology

journal homepage: www.elsevier.com/locate/jphotobiol

Green synthesis of NiO nanoparticles using *Aegle marmelos* leaf extract for the evaluation of in-vitro cytotoxicity, antibacterial and photocatalytic properties

A. Angel Ezhilarasi[a,b], J. Judith Vijaya[a,*], K. Kaviyarasu[c,d,**], L. John Kennedy[e], R. Jothi Ramalingam[f], Hamad A. Al-Lohedan[f]

[a] Catalysis and Nanomaterials Research Laboratory, Department of Chemistry, Loyola College, Chennai 600034, India
[b] Department of Chemistry, Jeppiaar Engineering College, Chennai 600119, India
[c] UNESCO-UNISA Africa Chair in Nanosciences/Nanotechnology Laboratories, College of Graduate Studies, University of South Africa (UNISA), Muckleneuk Ridge, P O Box 392, Pretoria, South Africa
[d] Nanosciences African network (NANOAFNET), Materials Research Group (MRG), iThemba LABS-National Research Foundation (NRF), 1 Old Faure Road, 7129, P O Box 722, Somerset West, Western Cape Province, South Africa
[e] Materials Division, School of Advanced Sciences, Vellore Institute of Technology University, Chennai Campus, Chennai 600127, India
[f] Surfactant Research Chair, Chemistry Department, College of Science, King Saud University, Riyadh 11451, Saudi Arabia

ARTICLE INFO

Keywords:
NiO
Green synthesis
Photocatalytic degradation
Cytotoxicity
Antibacterial activity
Biomedical application

ABSTRACT

In the present study, we report the green synthesis of NiO nanoparticles using *Aegle marmelos* as a fuel and this method is ecofriendly and cost effective. The plant *Aegle marmelos* is used in the field of pharmaceuticals to cure diseases like chronic diarrhea, peptic ulcers and dysentery in India for nearly 5 centuries. The as-prepared nanoparticles were confirmed as pure face centered cubic phase and single crystalline in nature by XRD. The formation of agglomerated spherical nanoparticles was shown by HR-SEM and HR-TEM images. The particle size calculated from HR-SEM was in the range 8–10 nm and it matches with the average crystallite size calculated from the XRD pattern. NiO shows intense emission peaks at 363 and 412 nm in its PL spectra. The band gap of 3.5 eV is observed from DRS studies and the formation of pure Ni—O is confirmed by FT-IR spectra. The as-prepared NiO nanoparticles show super paramagnetic behavior, when magnetization studies are carried out. It is then evaluated for cytotoxic activity towards A549 cell culture, antibacterial activity and photocatalytic degradation (PCD) of 4-chlorophenol (4-CP), which is known as the endocrine disrupting chemical (EDC). From the results, it is found that the cell viability of A549 cells was effectively reduced and it showed better antibacterial activity towards gram positive bacterial strains. It is also proved to be an efficient and stable photocatalyst towards the degradation of 4-CP.

1. Introduction

The increasing environmental pollution has attracted the world wide researchers to work on the development of efficient photocatalysts based on semiconductors for the treatment of contaminated water resources by various organic pollutants that are released from many industries [1]. They impart toxic damage to the environment, human body and aquatic life [2]. Various methods were employed for water treatment like reverse osmosis, active sludge, coagulation and electrochemical oxidation, but most of the organic dyes persist in water even after treatment, because of their stability against temperature, light and chemicals. In recent research, photocatalytic degradation has been suggested as the inexpensive method to remove the organic dyes and pollutants from waste water by using metal oxide semiconductors like ZnO, TiO_2, CuO and NiO [3,4]. Among the semiconductors in nanoregime, the unique features of NiO like inexpensive, non-toxic, photostability and easy availability make it to be an efficient photocatalyst for the degradation of various organic pollutants [5]. In the past few decades, the research efforts to combat the negative effects of EDCs have grown immensely, since they have to be completely removed from the sewage at water treatment plants before the final release into the environment. In recent days, EDCs like 4-CP enter waterways as

* Corresponding author.
** Corresponding author at: UNESCO-UNISA Africa Chair in Nanosciences/Nanotechnology Laboratories, College of Graduate Studies, University of South Africa (UNISA), Muckleneuk Ridge, P O Box 392, Pretoria, South Africa.
E-mail addresses: judithvijaya@loyolacollege.edu (J. Judith Vijaya), kavi@tlabs.ac.za (K. Kaviyarasu).

https://doi.org/10.1016/j.jphotobiol.2018.01.023
Received 10 October 2017; Received in revised form 20 January 2018; Accepted 22 January 2018
1011-1344/ © 2018 Elsevier B.V. All rights reserved.

solvents, insecticides, fungicides, herbicides and plasticizers through industrial, medical, agricultural and domestic activities, thereby causing a serious threat to the environment. Because of a new emerging pathogens and the resistance developed against antibacterial therapy, a serious research is needed for the development of efficient antimicrobial agents [6]. Development of multiple drug resistance conventionally has led to adverse side effects, hence, there is an emerging need for alternative strategies to treat bacterial diseases. Nowadays, nanoscale antimicrobial agents and nanosized carriers for antibiotics delivery have been developed and they have proven their effectiveness for treating infectious diseases in vitro and animal models [7]. NiO nanoparticle is known for its antimicrobial activity against various bacterial pathogens and also as an effective photocatalyst in the removal of dyes and organic pollutants from waste water [8]. It is also good in imparting cytotoxic activity over various cells like human airway epithelial (HEp-2) and human breast cancer (MCF-7) cells.

In recent research, nickel oxide nanoparticles have drawn a greater interest, because of its unique properties. It belongs to a wide band gap (3.6–4.0 eV) p-type semiconductor and is chemically stable with high electro-optical efficiency. Nickel oxide nanoparticles are widely applied in numerous fields as adsorbents, solar and fuel cells, catalytic agents, gas sensors, magnetic and antibacterial materials [9,10]. Since particle size, morphology and high crystallinity influence the physiochemical properties, it is of great importance to synthesize NiO nanoparticles with small particle size, preferably less than 20 nm, which could enhance the efficiency of their applications [11].

The nanomaterials having unique properties are used in various applications, such as photocatalysis, lithium ion batteries, smart windows, field emission studies, antimicrobial activity, dye-sensitized photocathodes, thermal conductivity and anti-ferromagnetic films [12–15]. Because of the peculiar physiochemical properties, the nanoparticles change the properties of the materials like its thermal, optical, electrical and mechanical properties [16]. The methods like coprecipitation, microemulsion, sol-gel method, electrospray synthesis, laser ablation and hydrothermal reaction [17–18] are used for the synthesis of nanomaterials. These conventional methods possess high cytotoxicity, low productivity and are not ecofriendly. In the past few decades, bionanotechnology is gaining momentum, as the scheme includes non-hazardous, environmental friendly biological systems like bacteria, fungi, leafs, vitamins and yeast for the synthesis of metal oxide nanoparticles [19]. Hence in the present work, NiO nanoparticles are prepared by a novel, simple, efficient, environment friendly and green route using *Aegle marmelos* extract, which plays the role of reducing, capping agent and fuel. It is also reported that using leaf extract, it is possible to control the shape and size of the particles. Being biotemplates, it also hinders agglomeration of nanoparticles [20].

Aegle marmelos, commonly known as Bilva or Sriphal or Bael are indigenous to India for over 5000 years. It is found in abundance in the Himalayan regions, Bengal, Srilanka, Burma, Vietnam and Pakistan. The root, bark, seed and fruit of *Aegle marmelos* are of great value in the folk systems and the traditional ayurvedic system of medicine in India. The fruit pulp of *Aegle marmelos* contains bioactive compounds like phenolics, alkaloids, pectins, flavonoids, tannins, coumarins, carotenoids and terpenoids [21]. The leaves also possess astringent and febrifuge properties, which are useful in treating dropsy, diarrhea, dysentery and bowel complaints. *Aegle marmelos* is reported to contain major phytochemicals, such as, limonene, bphellandrene, p-cymene, linalool, a-cubebene, 3,5-octadiene-2-one, trans-p-mentha-2,8-dienol, citronellal, cineole, citronella, citral, cuminaldehyde, β-cubebene, β-caryophyllene, hexadecane, pulegone, α-humulene, verbenone, carvone, carvylacetate, dihydro-β-ionone, (E)-6,10-dimethyl5,9-undecadien-2-one, β-ionone, caryophyllene oxide, humulene oxide and hexadecanoic acid [22].

Aegle marmelos has a broad range of therapeutic effects, namely inhibition of lipid peroxidation, anti-diarrheal, antioxidant, antibacterial, antiviral, anti-ulcerative colitis, cardio protective, antidiabetic, gastro protective and radio protective effects. The *Aegle marmelos* leaves possess antibacterial and antifungal activities in vitro. The infections in humans, especially in children caused by coxsackie viruses B1–B6 and the antiviral effects are reported by Badam et al. [23]. In recent years different types of fuels are used in the combustion synthesis which includes polyethylene glycol (PEG), poly-acrylic acid (PAA), organic polymers, starch-derived polymer and many more. During combustion these fuels decompose with the emission of large amount of heat and toxic gases. As a viable alternative to chemical synthetic procedures plant extracts are employed in the synthesis of nanomaterials, as reducing and capping agents. In our present study, we have used the leaf extract of *Aegle marmelos* as the fuel to syntheses NiO nanoparticles and evaluate their efficiency in terms of cytotoxicity, antibacterial activity and photodegradation of 4-CP. Since records of *Aegle marmelos* prove that they contain important bioactive compounds which initiated antibacterial effects on various pathogens and have also been used as an adsorbent for the removal of toxic metal in preventing the environment, it would be a promising fuel in synthesizing NiO nanomaterial.

2. Experimental Method

2.1. Preparation of Nickel Oxide Nanoparticles Using Aegle marmelos Leaves by Hot Plate Combustion Method

Aegle marmelos leaves were taken and washed thoroughly with distilled water. They were then cut into pieces and ground using pestle and mortar. From this, 30 g of leaves was stirred in 100 mL of distilled water and ethanol for 2 h. It is then kept for incubation for 24 h at room temperature. Finally, it was filtered using Whatmann No.1. filter paper. The clear solution obtained is the plant extract, which is used as a fuel to synthesize NiO nanoparticles.

The hot plate combustion method was employed to synthesize NiO nanoparticles from 0.1 mM $Ni(NO_3)_2$ aqueous solution (Merck chemicals, India, 99% purity), *P. Aegle marmelos* leaf extract (5 mL) and glycine ($C_2H_5NO_2$). The amount of precursor for the synthesis was estimated using the stoichiometric ratio and 1.5 g of NiO was obtained. Initially, the precursors were dissolved in a 70 mL of deionized water and kept aside for 1 h with continuous and constant stirring to attain a homogenous mixture of a solution. In the hot plate combustion method, the above homogeneous solution was placed in a hot plate heater (Barnstead Thermolyne, model no: SP46925) and uniformly heated up to 250 °C for 15 min, which leads to the volatilization of water and combustion of the reaction mixture. The black colored precipitate was then separated through centrifugation and washed multiple times with deionized water. The separated black powder was dried at 100 °C in hot air oven and subjected to annealing at 300 °C for 2 h.

2.2. Analytical Methods for Characterization

The formation of pure NiO phase was confirmed by Philips X'pert diffractometer for $2\theta = 10°–80°$, $\lambda = 0.154$ nm) and Perkin Elmer infrared spectrophotometer. The morphology and particle size was observed by stereoscan LEO 440 (HR-SEM) and (JEOL 3010) (HR-TEM). Cary100 UV–Visible spectrophotometer and Varian Cary Eclipse Fluorescence Spectrophotometer were used to study the absorption and emission properties of NiO nanoparticles. Structural characterization of the synthesized nickel oxide nanoparticles prepared using *Aegle marmelos* leaf extract was performed using Philips X'pert diffractometer for $2\theta = 10°–80°$ using Cu Kα radiation at $\lambda = 0.154$ nm. The surface functional group of NiO nanoparticles was determined by Perkin Elmer infrared spectrophotometer. The particle size and morphology were performed using high resolution scanning electron microscope (HR-SEM) (Stereoscan LEO 440) and high resolution transmission electron microscope (HR-TEM) (JEOL 3010). Absorption and emission characteristics of the synthesized photocatalysts were recorded using Cary100 UV–Visible

spectrophotometer and Varian Cary Eclipse Fluorescence Spectrophotometer at an excitation wavelength of 372 nm.

2.3. In-vitro Cytotoxic Activity NiO Nanoparticles by MTT Assay

Nano NiO prepared using *Aegle marmelos* leaf extract was evaluated for in-vitro cytotoxic activity against A549 cell lines (Life Tech Research Center, Chennai). Cells were maintained at humid atmosphere with 5% CO_2 after seeding in a 96-well plate at 37 °C. It was kept for incubation for 24 h and then the culture medium was removed. The mitochondrial activity of the cultured cells were determined using 3-(4,5-dimethyl-2-thiazolyl)-2,5-diphenyltetrazolium bromide (MTT) assay and the degree of cytotoxicity was evaluated for various concentrations of the synthesized NiO nanomaterial and the range of extracts added to the culture medium were 1000, 500, 250, 125, 62.5, 31.2, 15.6 and 7.8 μg/mL. The mitochondrial succinate dehydrogenase enzymes in the viable cells reduced MTT, a yellow dye into purple colored formazan crystals, which were further dissolved in DMSO to attain the complete solubility. Later the optical density for various concentrations was quantified by using the spectrophotometer at specified wavelength.

2.4. Antibacterial Activity Studies

The antibacterial activity of the NiO nanoparticles was evaluated against both Gram positive (*Streptococcus Pnemoniae*, *Staphylococcus aureus*) and Gram negative (*Escherichia Hermannii*, *Escherichia coli*) bacterial strains and the test organisms were collected from American type culture collection (ATCC) and Microbial type culture collection (MTCC) Chandigarh, India. Disc diffusion method was employed to study the antibacterial behavior of NiO nanoparticles. Petri plates were prepared with 20 mL of sterile Muller Hinton agar (MHA, Himedia) and each bacterial pathogen was individually swabbed on MHA in separate plates. The antibacterial activity was tested at a specific concentration with the required quantity of the NiO nanoparticle dissolved in dimethyl sulphoxide (DMSO). The zone of inhibition levels (mm) were measured after 24–48 h and before this step, it was incubated overnight at 37 °C. The sample loading was carried out by Kirby Bauer method.

2.5. Photocatalytic Reactor Setup and Degradation Procedure

The schematic diagram of the photocatalytic reactor is shown in Fig. 1. The degradation studies were done by using a photocatalytic reactor designed by us for the study. It has quartz/borosilicate cylindrical tubes with dimensions 36–1.6 cm (height-diameter). After the optimization, optimum 4-CP solution and NiO nanoparticles (photocatalysts) were taken in the above mentioned reactor tubes supported with air passage, so that the photocatalyst is exposed to the irradiated light throughout the reaction. It is irradiated with UV light using a low pressure mercury lamp that emits light of wavelength at 365 nm. In the present study, 100 mL of aqueous 4-CP was taken along with optimum NiO catalysts and kept for stirring for 30 min. It was aerated for 30 min and then subjected to UV light. Aliquots were withdrawn at specific intervals of time from the suspension, centrifuged (1500 rpm) and filtered using 0.2 μm Millipore filter paper. The rate of degradation of 4-CP was monitored using Perkin Elmer UV–Visible spectrophotometer.

The expression given below is used to calculate the degradation efficiency (η);

$$\eta = Ci–Ct/Ci \text{ X } 100.$$

where Ci and Ct are the initial concentration and concentration of 4-CP after "t" minutes respectively.

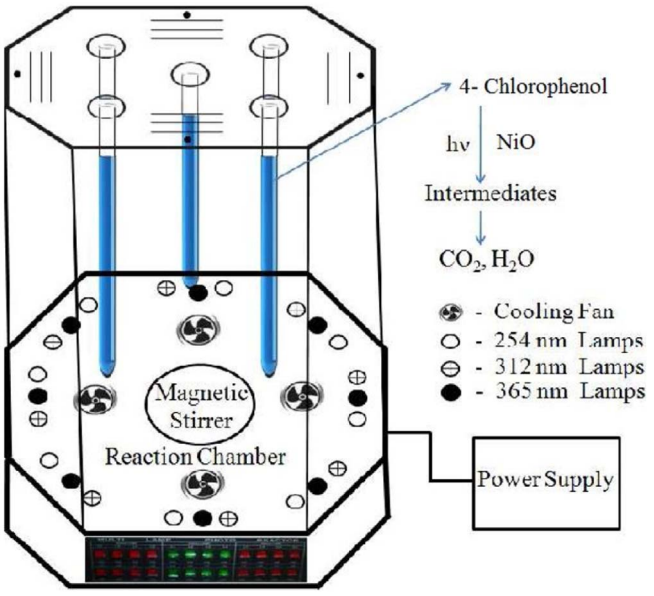

Fig. 1. Schematic diagram of the photocatalytic reactor.

3. Results and Discussion

3.1. Structural Investigations of NiO Nanoparticles Prepared Using Aegle marmelos Leaf Extract

Fig. 2 shows the XRD pattern of the synthesized NiO nanoparticles using *Aegle marmelos* leaf extract prepared by the hot plate combustion method. The highly crystalline NiO nanoparticles displayed sharp and intense diffraction peaks that perfectly matched well with the standard JCPDS file no: 4-0835. It shows the presence of (111), (200), (220), (311) and (222) planes. The XRD pattern confirms the formation of pure face centered cubic NiO and the broad peaks correspond to the presence of oxygen vacancies and local lattice disorder in the sample [24]. The leaf extract used acts as a fuel to produce nanoparticles in nanoregime having high surface area and good dispersity. The crystallite size was estimated from the plane (200) and is found to be 8.15 nm, and this may be due to the presence of various photochemicals in the *Aegle marmelos* leaf extract, which plays the role of fuel, capping and reducing agents so that nanometal oxides are formed [25]. This is the favorable condition towards their biological and photocatalytical activity.

The surface morphology of the as-synthesized NiO nanomaterial prepared using *Aegle marmelos* leaf extract was studied using HR-SEM images as shown in Fig. 3. The particles were cubic and spherical in shape with slight agglomeration. The formation of nanoparticles is due

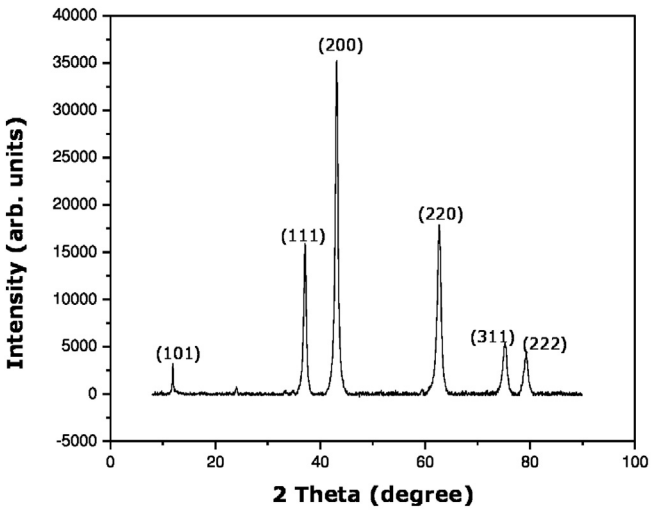

Fig. 2. XRD pattern of NiO nanoparticles prepared using *Aegle marmelos* plant extract.

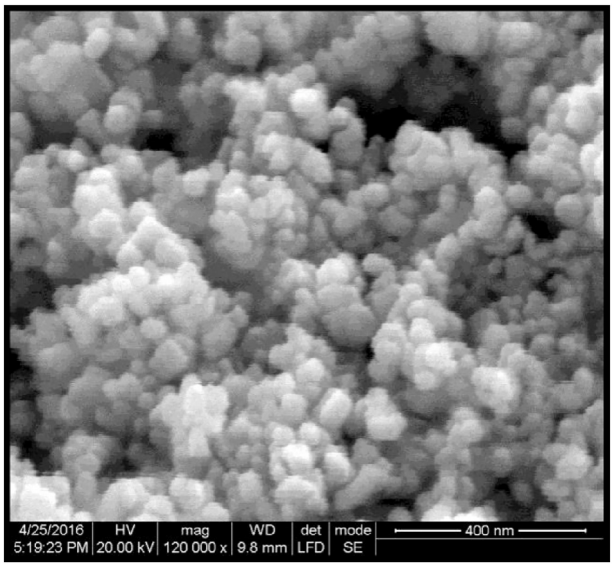

Fig. 3. HR-SEM image of NiO prepared using *Aegle marmelos* plant extract.

to the large volume of heat produced during the combustion process. The amount and nature of the fuel used forms the size, shape, morphology, degree of agglomeration and properties. The formation of cubic and spherical nanoparticles which are slightly agglomerated and porous was observed in HR-TEM images (Fig. 4). The corresponding selected area electron diffraction (SAED) shows polycrystalline nature. The particle size was in the range of 8–10 nm and it agrees well with the average crystallite size calculated from the XRD pattern. The agglomeration of particles confirms the presence of polymeric adherence and magnetic interaction among the particles [26]. The *Aegle marmelos* leaf extract, which acts as a fuel is capable of producing NiO nanoparticles and therefore act as a promising fuel to prepare the nanomaterials. The purity of NiO nanoparticles was confirmed by Energy Dispersive X-ray analysis (EDX), which accurately quantified the Ni and O contents by showing only Ni and O peaks without any other impurity (Fig. 5). It is the supporting evidence for the formation of pure NiO along with XRD and FT-IR studies.

3.2. Photoluminescence Investigations of NiO nanoparticles Prepared Using Aegle marmelos Leaf Extract

The nanostructured materials possess high density of crystal defects than their bulk. The PL spectra was recorded to understand the effects of quantum size and crystal defects. Fig. 6 shows the PL spectra with intense emissions peaks at 363 nm, 412 nm and broad emission near 440 nm. The radiative recombination of the excited electrons with the holes in the valence band is confirmed by the UV emission at 363 nm. Due to the presence of

Vo and *Ni*(in) defects there is an emission peak at 412 nm, which in turn confirms the intrinsic defects. The presence of shoulder peak near 440 nm [27,28] corresponds to the surface defects. Hence the *Aegle marmelos* leaf extract used in the present study was able to synthesize NiO nanomaterials with intrinsic defects, oxygen vacancies and surface defects, which will usually enhance the photocatalytic and biological

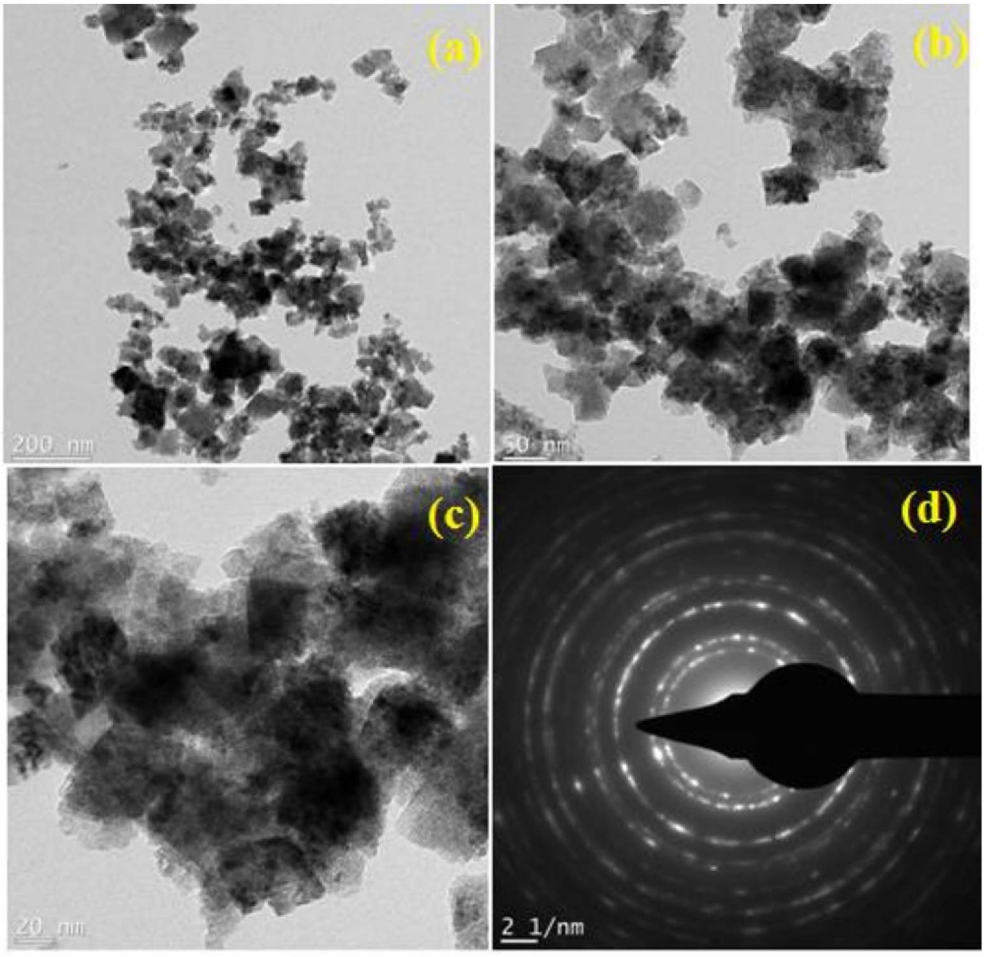

Fig. 4. (a, b, c, d). HR-TEM images of of NiO nanoparticles prepared using *Aegle marmelos* plant extract.

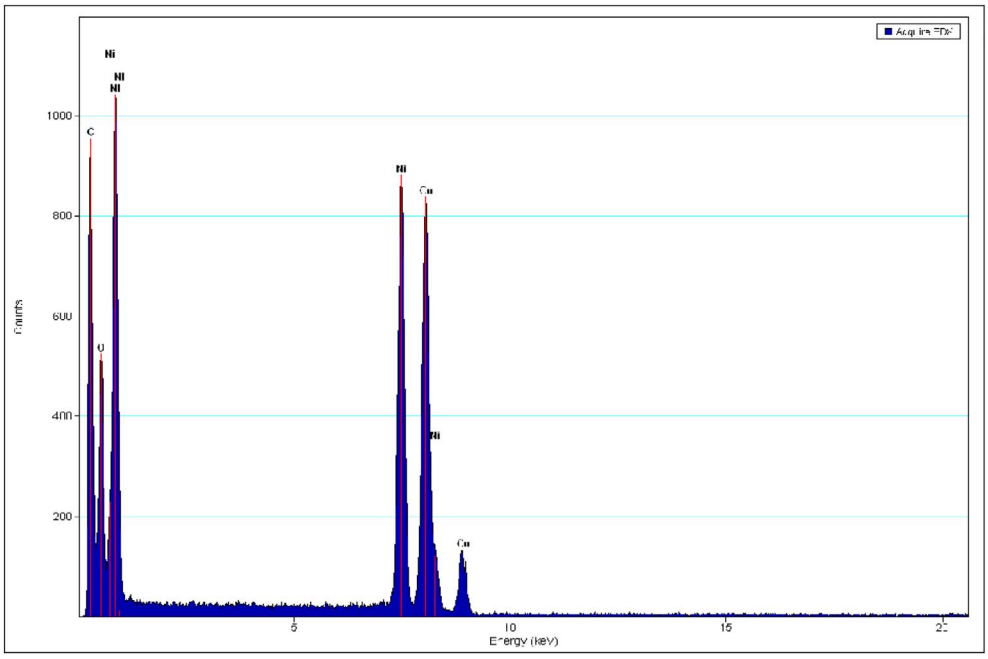

Fig. 5. EDX spectrum of NiO nanoparticles prepared using *Aegle marmelos* plant extract.

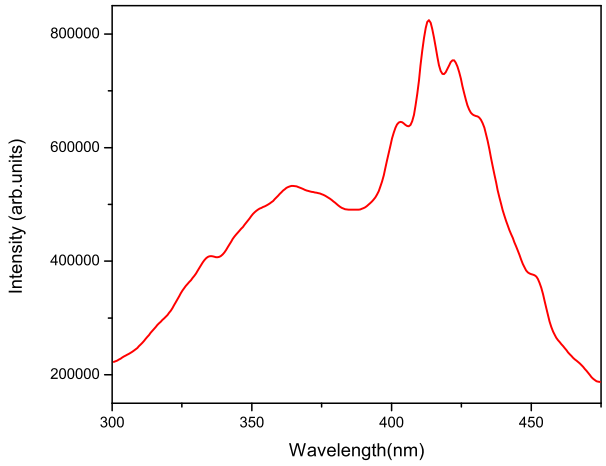

Fig. 6. PL spectra of NiO nanoparticles prepared using *Aegle marmelos* plant extract.

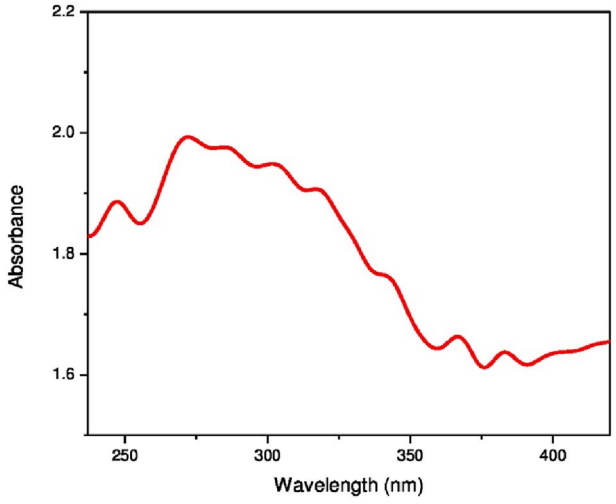

Fig. 7. UV–visible diffuse reflectance spectra of NiO nanoparticles.

activity. Hence, it is believed that the synthesized NiO nanomaterial with reduced particle size, high surface defects and high surface area will possess enhanced activity.

3.3. DRS Studies

Fig. 7 shows the optical diffuse reflectance spectra (DRS) recorded at room temperature using Teflon as a reference sample to calculate the energy band gap of NiO nanoparticles. There is a small band at 247 nm (5.02 eV) and a broad band in the range of 269–346 nm (4.60–3.58 eV). Generally NiO displays an optical band gap of 3.5 eV and the absorption peak at 355 nm. Hence, the absorption peaks at 303 nm, 371 nm and 341 nm may be due to the quantum confinement. The electronic transition from the ionized oxygen vacancies to the valence band of NiO originated from the surface defects occurs below 300 nm. Therefore the increased band gap of the synthesized NiO nanomaterial than that of the bulk indicates the reduced particle size of the NiO nanomaterial and the existence of quantum confinement effect. However, the absorption peak of the NiO nanomaterial is at lower energy in the UV region than that of the bulk, hence it could be potentially used as a photocatalyst,

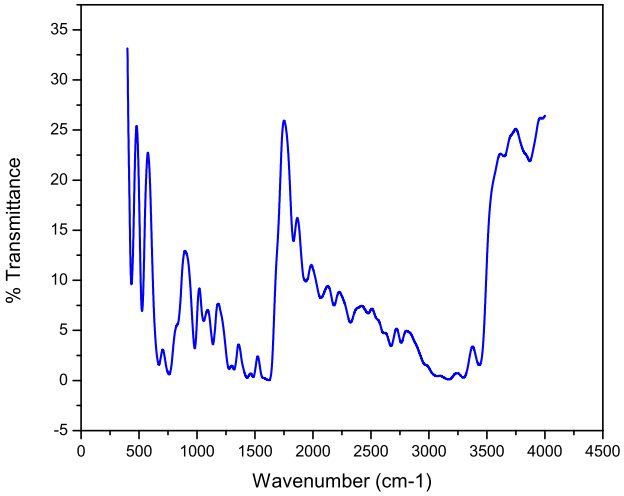

Fig. 8. FT-IR spectra of NiO nanoparticles prepared using *Aegle marmelos* plant extract.

since the excitation of electrons from the valence band to the conduction band is possible through UV light excitation.

3.4. Fourier Transform Infrared Spectroscopy (FT-IR) Studies

Fig. 8 shows the FT-IR spectra of NiO nanoparticles prepared using *Aegle marmelos* leaf extract. The strong intense peaks at 482 cm^{-1}, 580 cm^{-1} and 900 cm^{-1} confirm the presence of metal oxygen stretching frequency of Ni-O in the synthesized nanoparticles [29]. The moderate peak observed at 1018 cm^{-1} corresponds to single C—O bond stretching mode. Absorption peaks observed at 1186 cm^{-1}, 1356 $cm^{-1}$and 1518 cm^{-1}corresponds to C═C aromatic stretching vibration band, which may be due to various phytochemicals present in the *Aegle marmelos* leaf extract. The broad band at 3400–3700 cm^{-1} is because of the stretching vibration mode of the chemically bonded hydroxyl group, and it is due to the water molecules adsorbed on the surface of NiO. The adsorption of water molecules by the nanoparticles indicate that the synthesized nanomaterial possess high surface area [30]. The presence of carbonyl group in the leaf extract is confirmed by the strong intense peak at 1750 cm^{-1} and the moderate peak 3380 cm^{-1} is due to the N—H (amine) stretching frequency [31]. Thus, the results of FT-IR spectrum coincide with the XRD data and in turn confirm the formation of highly pure single NiO nanoparticles.

3.5. Magnetization (VSM) Studies

The magnetization behavior of the synthesized NiO using *Aegle marmelos* leaf extract was investigated by sweeping the external magnetic field between + 20 kOe to − 20 kOe at 300 K. Fig. 9 shows the plot between magnetization (M) Vs magnetic field (H). The NiO exhibited slight curves in the low magnetic field, and a linear portion at higher magnetic field regions. It was also observed that the sample never attained saturation even at higher magnetic field of about (20 kOe), which confirms the presence of super paramagnetism. If there is a reduction in the particle size, the magnetic property will be changed from diamagnetism to super paramagnetism [32]. Hence the super paramagnetic behavior exhibited is due to the reduced particle size (8.15 nm) [33], which are also proven by the obtained XRD results. As the magnetic behavior is sensitive towards the magnetic impurities, the existence of super paramagnetic behavior even at higher magnetic field proves the purity of the sample. The methodology employed in synthesizing NiO nanoparticles using phytochemicals in the present work has resulted in reduced particle size with super paramagnetic behavior, and in turn proves to be a promising material for various magnetic applications.

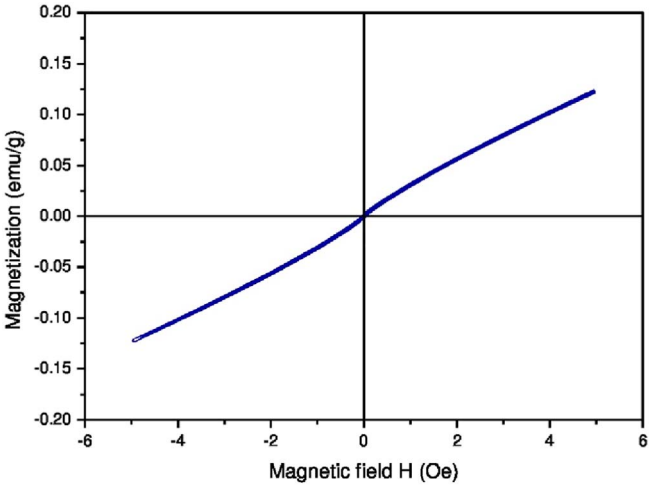

Fig. 9. Magnetic hysteresis (M–H) curves measured at 300 K for NiO nanoparticles.

Table 1
MTT assay measurement of % Cell viability and Absorbance for various concentrations of NiO nanoparticles prepared using *Aegle marmelos* leaf extract.

S. No	Concentration (μg/mL)	Dilutions	Absorbance (O.D)	Cell viability (%)
1	1000	Neat	0.103	20.11
2	500	1:1	0.187	36.52
3	250	1:2	0.225	43.94
4	125	1:4	0.264	51.56
5	62.5	1:8	0.293	57.22
6	31.2	1:16	0.312	60.93
7	15.6	1:32	0.324	63.28
8	7.8	1:64	0.331	64.64
9	Cell control	–	0.512	100

3.6. Evaluation of In Vitro Cytotoxicity Activity Using NiO nanoparticles prepared using Aegle marmelos leaf extract

The cytotoxic effect of the synthesized NiO nanoparticles was evaluated for A549 cell line. The diluted ranges of synthesized NiO extracts added to each plates were 1000, 500, 250, 125, 62.5, 31.2, 15.6 and 7.8 μg/mL. The test samples was taken along with known quantity of the cells, and the % cytotoxicity for each concentration was tested by MTT (3-(4, 5-dimethyl-2thiazolyl)-2, 5-diphenyltetrazolium bromide) assay. The absorbance of the purple solution obtained by mixing the above crystals with dimethyl sulfoxide was measured at 540 nm using spectrophotometer [34]. The cytotoxicity was recorded using (IC50 value) the formula given below as the drug concentration causing 50% growth inhibition of the tumour cells.

$$\%cell\ viability = \frac{OD\ sample\ mean}{OD\ control\ mean} \times 100$$

Table 1 shows the variation of cell viability against various concentrations of the NiO nanoparticles. In general, the cell viability decreases with an increase in the concentration of nanoparticles and the percentage of reduction was dose dependant. In MTT assay, A549 cell viability was observed to be 20%, when treated with 1000 μg/mL of NiO nanoparticles prepared by *Aegle marmelos* leaf extract, and increased gradually to the maximum of 64.6% at the concentration of 7.8 μg/mL. The variation of the percentage cytotoxicity and optical density against various concentrations of NiO nanoparticles is shown in Fig. 10. The absorbance increases from 0.103 OD to 0.331 OD, since the NiO nanoparticle concentration is decreased from 1000 μg/mL to 7.8 μg/mL respectively, whereas for the controlled cells, the absorbance was 0.512 OD. From the results, it is confirmed that NiO nanoparticles have imparted a remarkable effect over A549 cells in cell damage, and it agrees well with the literature [35]. Fig. 11 shows the cell morphology of A549 cell lines treated against different concentration of NiO nanoparticles. From the image, it is clear that the morphology of A549 cell lines on treatment with the synthesized NiO nanoparticles has undergone cell swelling and cell damage as a result of apoptosis. In controlled cells, a smooth and regular morphology was observed and the intensity of cell line damage was dose dependent. It is evident from the figure that the cell line treated with 1000 μg/mL has a severe swelling and damage in the cell line. The mechanism for the influence of specific factors on the cytotoxic effects is not clear yet. There are few reports, which suggests that the metal ions released from the nanometal oxides play a major role in nanocytotoxicity [36]. The release of Ni^{2+} ions will be higher for nanosized NiO, which will induce a higher cytotoxicity than the micron sized particles. Hence, the higher cytotoxic activity of the synthesized NiO nanoparticles over A549 cell lines may also be attributed to their reduced particle size (8.15 nm). It favors the adsorption of proteins and salts on the surface and it can be related to the cellular influence [37,65–68]. The particle size of 8.15 nm achieved holds good agreement with TEM and XRD results. Metal ion release also supports the movement of the exogenous materials inside the cells and

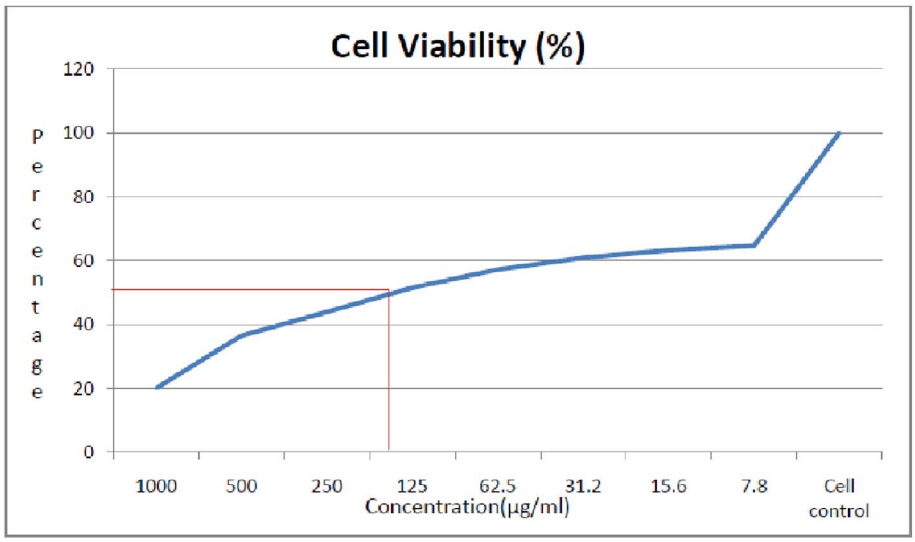

Fig. 10. MTT assay measurement on variation of % cell viability and optical density against various concentrations of NiO nanoparticles.

induces oxidative stress directly or indirectly. Different mechanisms were proposed based on the metal ions released. This includes the activation of calcium dependant and stress-inducible signaling cascades, which interferes with DNA repair pathways and causes epigenetic changes [38,39]. The excess production of reactive oxygen species ROS and oxidative stress can cause DNA damage and apoptosis. The oxidative stress may be because of the electrons transferred from the ROS like ·OH, H_2O_2·, O^{2}·$^{-}$ [40]. The above mentioned mechanism for the various damages due to the cell lines is shown in Fig. 12. The ROS produced damages cell wall of, DNA, single and double strand breaks and leads to severe cell death [41,69–71].

Thus the synthesized NiO nanoparticles using *Aegle marmelos* leaf extract as the fuel possess high cytotoxic activity and the results from Table 1 and Fig. 10 proves that at increased concentration of NiO nanoparticles, the absorbance and cell viability decreases. The reduced particle size, specific surface area and release of more Ni^{2+} ions cause maximum cytotoxic effect in the present study. Hence, NiO nanoparticles are promising biomaterial, since it induces cytotoxicity and apoptosis in A549 cell lines, which occurs through the generation of ROS and oxidative stress.

3.7. Evaluation of Antibacterial Activity

Antibacterial activity of the NiO nanoparticles synthesized by *Aegle marmelos* leaf extract was evaluated against two Gram positive and Gram negative strains. Various zones of inhibition (mm) are presented

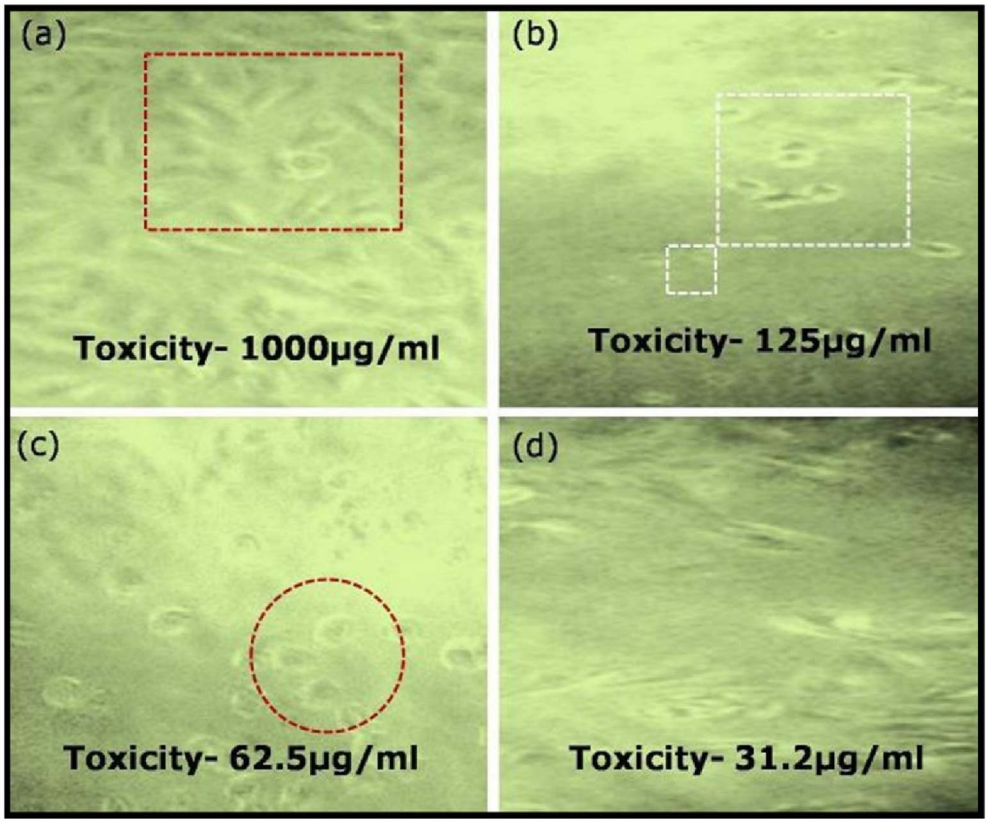

Fig. 11. (a, b, c, d) Effect of A549 cell morphology on treatment with NiO nanoparticles under various concentration.

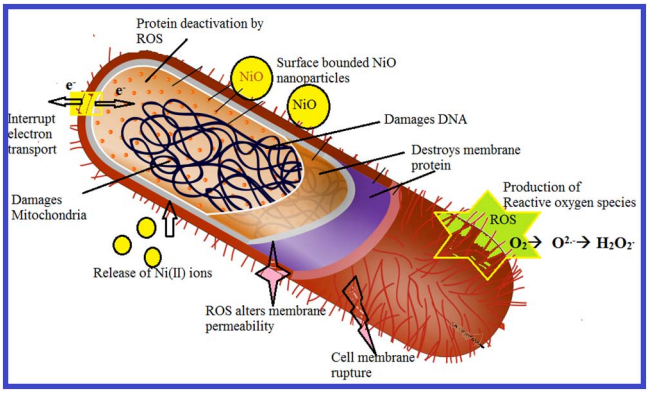

Fig. 12. Schematic mechanism of toxicity effect of NiO nanoparticles against bacteria.NiO nanoparticles and their ions generate ROS, and induce oxidative stress resulting in the damage of mitochondria, DNA, proteins and cell membrane with consequent cell death.

Table 2
Antibacterial activity of NiO nanoparticles against pathogens.

Bacterial strains	Zone of inhibition (mm)
Staphylococcus aureus	16
Streptococcus pnemoniae	12
Escherichia coli	11
Escherichia hermannii	6

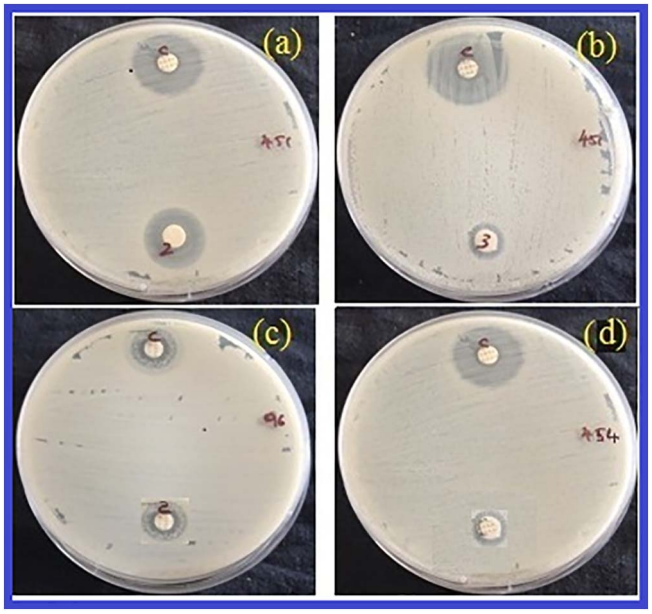

Fig. 13. Results of inhibition zones of antibacterial activity by NiO nanoparticles (a) *Staphylococcus aureus* - 16 mm (b) *Streptococcus pnemoniae* - 12 mm (c) *Escherichia coli* - 11 mm and (d) *Escherichia hermannii* - 6 mm.

in Table 2 and Fig. 13. It was observed that the as-synthesized NiO nanoparticles were more effective over Gram positive bacteria than the Gram negative bacterial strains *Staphylococcus aureus* (16 mm), *Streptococcus Pnemoniae* (12 mm), *Escherichia coli* (11 mm) and *Escherichia Hermannii* (6 mm). It is a well-known fact that the antibacterial activity will be more pronounced for Gram negative bacteria than Gram positive bacteria, because of the thin layer cell wall with single layer of peptidoglycan, whereas Gram positive bacteria possess multilayered thick peptidoglycan. There are also few reports on NiO nanoparticles that were more effective towards Gram positive bacterial strains [42,43].

The enhanced antibacterial activity is due to the smaller particle size of the NiO nanoparticle, as it enhances the dispersibility, and permits the inference of the extracellular Ni^{2+} with the intracellular Ca^{2+} metabolism, thus resulting in the cell damage. When the size of the nanoparticles decreases, the electrostatic interaction between the microbial cell membrane and Ni ions released from NiO nanoparticles becomes strong and hence increases the antibacterial activity [44]. The activity also depends on the stability, morphology, and shape of the nanoparticles for long term activity. In general, the effective antimicrobial activity depends on the particle dosage, methodology used and treatment time [45].

The exact mechanism of antibacterial activity is not reported yet, but there are studies that the nanoparticles interact with the bacteria by causing a change in the morphology of the membrane, thereby increases the permeability. It interrupts in the regular transportation through the plasma membrane, thus leading to cell death [46]. As the synthesized NiO nanomaterial has reduced particle size accompanied with large surface to volume ratio, it facilitates the interaction and enhances the antibacterial activity than the micron sized particles. Sulphur and phosphorus in the DNA of the bacteria and the functional groups of the protein interacts with NiO nanoparticles and leads to protein leakage and cell death [47].

The formation of ROS enhances the antibacterial activity and they are the natural by products of metabolism [48]. The cells are destroyed, because the induction of ROS that leads to the formation of highly reactive radicals, thereby damage the proteins, cell membranes, DNA, and intracellular system [49]. The schematic representation for the ROS· formation is shown in Fig. 14. When the light is incident on NiO nanomaterial, whose photon energy is higher than the band gap Eg, because of the photoexcitation there will be a formation of holes (h^+) in the valence band and electrons (e^-) in the conduction band. They have high redox properties and hence react with molecular oxygen (O_2) and hydroxyl ions (·OH) to generate various ROS·. When molecular oxygen traps the electron, it generates superoxide anion ($O^{2\cdot -}$), hydrogen peroxide (H_2O_2·) and hydroxyl radicals (•OH). Superoxide anion reacts with water molecules and there will be absorption of electrons from water and hydroxyl ions from the holes for the mineralization of bacterial cells. The production of ROS· is mandatory and they are the dominant species to decide the cell death, since it induces oxidative stress, and lead to the damage of cell membrane, protein deactivation, interrupt in the electron transport, damages DNA and mitochondria, and thus results in cell death [50].

Hence, in the present study, the antibacterial activity is enhanced, because of the use of NiO having high stability, smaller size and spherical morphology and this is because of the usage of *Aegle marmelos* leaf extract by a green route. The sufficient amount of Ni^{2+} ions released penetrate into the cell wall, which later disturb the electron transport and affect DNA, protein and mitochondria, which finally leads

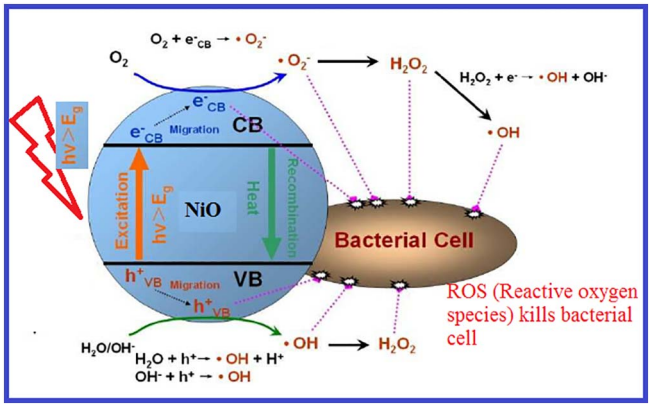

Fig. 14. Schematic representation of the light irradiated NiO nanoparticles and the generation of ROS causing bacterial death.

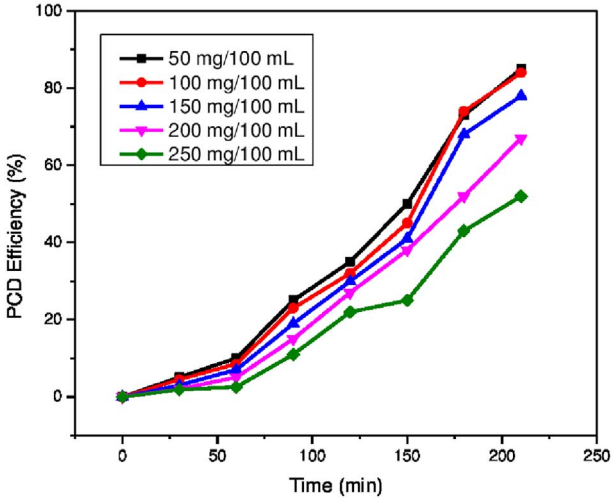

Fig. 15. Effect of concentration of 4-CP on PCD efficiency. Experimental conditions: [NiO] = 30 mg/100 mL, initial pH of suspension = 6.5 (natural pH), λ = 365 nm.

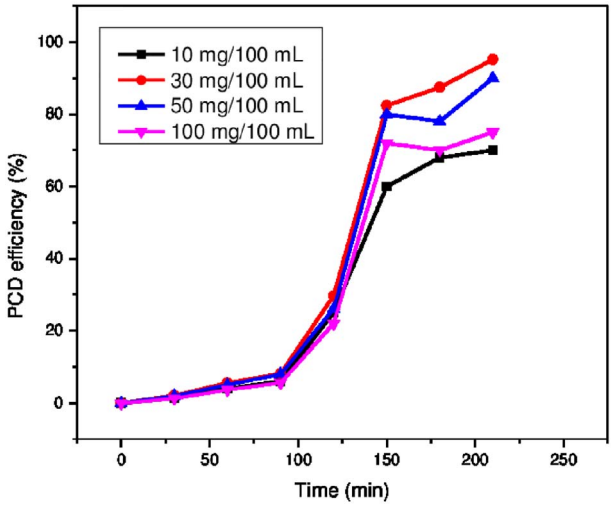

Fig. 16. Effect of the amount of photocatalyst on PCD efficiency. Experimental conditions: catalyst = NiO, [4-CP] = 100 mg/L, initial pH of suspension = 6.5(natural pH), λ = 365 nm.

to the cell death. As a result of natural metabolism, there is a generation of ROS under light irradiation. Oxidative stress is induced inside the cell that results in cell death. Since the activity and stability of NiO nanoparticles are effective, they could be employed in as antimicrobial coatings that will be helpful for various environmental and biomedical applications.

3.8. Photocatalytic Degradation of 4-CP

3.8.1. Effect of the Concentration of 4-chlorophenol

50–250 mg/L of the 4-CP was considered at a neutral pH to study the effect of initial concentration on the photocatalytic degradation (PCD) (Fig. 15). The PCD efficiency decreased from 93% to 74%, when the initial concentration of 4-CP is increased from 50 to 250 mg/L. It may be because of the adsorption of more and more 4-CP molecules on the surface of NiO and the amount of ·OH and $\cdot O^{2-}$ radicals may be insufficient to degrade higher concentration of 4-CP [51]. There may be a production of more intermediates, which will compete to react with ·OH formed from photo generated holes [52]. Hence, under the given set of conditions, the maximum concentration of 4-CP that could be photodegraded by 30 mg/100 mL of NiO nanoparticles is found to be 100 mg/L. Thus, 100 mg/L 4-CP was fixed as the optimum concentration for the study of other parameters.

3.8.2. Effect of the Catalyst Dosage

In order to investigate the optimum amount of catalyst needed for the efficient PCD of 4CP, the catalysts dosage was varied as shown in Fig. 16. The results indicate that a maximum PCD occurs for 30 mg/100 mL, which confirms that the rate of photodegradation is affected by the total number of available active sites of the catalyst and photo absorption ability. With increased catalyst dosage, the PCD is decreased because it prevents the illumination of UV light and affects the production of hydroxide radicals, which are primary oxidants in the photo degradation process and high catalyst dosage also induces scattering effect. Thus, 30 mg/100 mL of NiO nanoparticle was fixed as the optimum catalyst dosage to study the mineralization of 4CP.

3.8.3. Effect of Initial pH

The PCD efficiency was studied under different pH [4,6,8,10] under the optimized experimental conditions (100 mg/L 4-CP solution and 30 mg/100 mL NiO nanoparticle loading) shown in Fig. 17. When pH = 2, the PCD of 4-CP was found to be very low and with an increase in pH the efficiency of PCD also increased and maximum PCD is observed at pH = 8, which later decreased at pH = 10. In acidic medium,

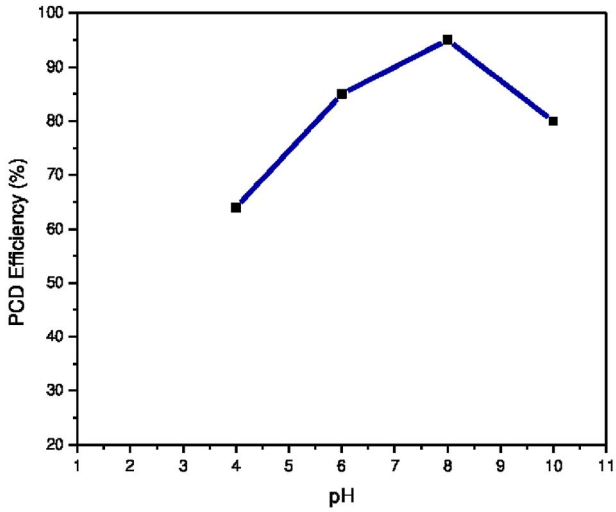

Fig. 17. Effect of pH on PCD efficiency. Experimental conditions: Catalyst NiO = 30 mg/100 mL, [4-CP] = 100 mg/L, λ = 365 nm).

the reduced PCD of 4-CP is due to the significant loss of NiO to Ni^{+2} [53] which in turn reduces the production of ·OH. In alkaline medium, there will be a production of more ·OH radicals, the primary oxidizing agent which will enhance PCD [54], Also the stability of NiO nanoparticles was not disturbed under the alkaline conditions, which favors the adsorption of 4-CP on the surface and leads to increased PCD efficiency. At pH = 10, the decrease of PCD is attributed to the negative charge on NiO surface, which reduces the concentration of 4-CP. The formation condition occurs at a pH, where the surface charge becomes zero so that there will be a generation of more ·OH radicals and adsorption of more 4CP molecules on the catalyst surface [55]. Consequently, the PCD was effective till pH = 9 and decreased at pH = 10. Hence, the optimum pH is considered as pH = 8.

3.8.4. Photocatalytic Mineralization of 4-CP

The photocatalytic degradation of 4-CP was carried out under optimized conditions (4CP = 100 mg/L, photocatalyst = 30 mg/100 mL, pH = 8, NiO nanomaterial) at the wavelength of 365 nm. The irradiation of UV light on the photocatalyst promotes the electrons to the conduction band with high kinetic energy and there is a formation of holes in the valence band. The effect of time on PCD efficiency of 4-CP

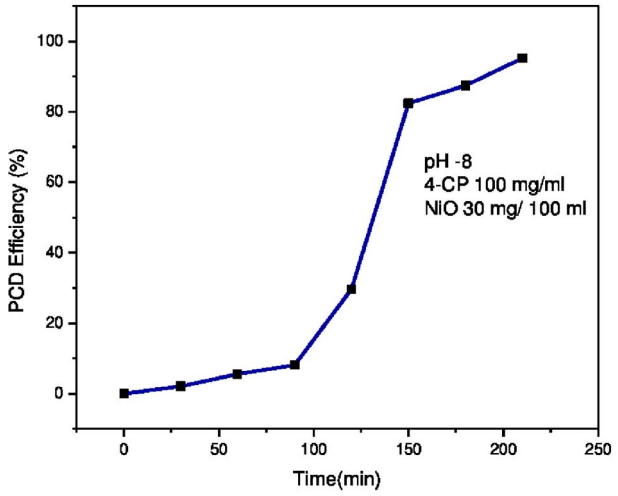

Fig. 18. Degradation efficiency of NiO. Experimental conditions: [4-CP] = 100 mg/L, [catalyst] = 30 mg/100 mL, pH = 8, λ = 365 nm, irradiation time – 210 min.

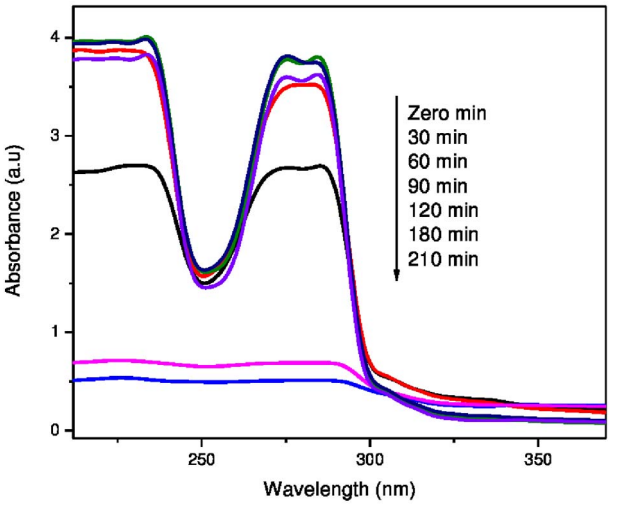

Fig. 19. UV – Vis absorption spectra of the photocatalytic degradation of 4-CP. Experimental conditions: irradiation wavelength λ = 365 nm, [4-CP] = 100 mg/L, [catalyst NiO] = 30 mg/100 mL.

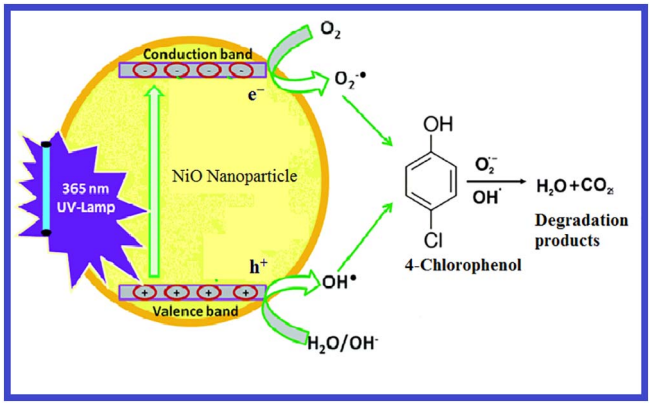

Fig. 20. Schematic representation for the degradation of 4-CP on UV light irradiation.

is shown in Fig. 18. UV–Vis spectrophotometer is used to analyse the experiments that were conducted batch wise. Fig. 19 represents the degradation spectra of 4-CP recorded by UV–Vis spectrophotometer. From the results, it is found that the mineralization of 4-CP is less than 1% at 90 min, which increased rapidly to 87% at 180 min and complete mineralization is observed at 210 min. The presence of few long lived intermediates would have caused the slow degradation initially. Later, the PCD is initiated by branch dissociation, where ·OH reacts with the organic molecules (4-CP) on the catalytic surface [56]. The possible degradation mechanism scheme is shown in Fig. 20. When NiO is irradiated by light having the greater band gap energy, there will be an electron excitation from the valence band [VB] to a conduction band [CB], thereby leaving a hole in the valence band. The electrons at the conduction band absorb molecular oxygen and produces $\cdot O^{2-}$ and the holes in VB forms ·OH by reacting with water [57]. OH· being the powerful oxidizing agent degrade the organic pollutants on the photocatalytic surface. In the present work, the efficient and complete mineralization of 4-CP occurs, which is due to the reduced particle size of NiO [58–62]. Photocatalytic nanoparticles with smaller particle size possess more active sites and exhibit high efficiency in surface charge carrier transfer [63–64]. Furthermore, the synthesized nanomaterial was capable of absorbing light on irradiation with the production of sufficient amount of hydroxide, superoxide and peroxide radicals to mineralize 4-CP completely to CO_2 and H_2O. Thus the synthesized NiO nanomaterial using *Aegle marmelos* leaf extract possess unique features like spherical self-assembled morphology, reduced particle size inherent with surface defects, high crystallinity and stability. From all the above results, it is concluded that NiO nanoparticles prepared in the present study can be used in waste water treatment and it helps to reduce the environmental pollution.

4. Conclusion

Aegle marmelos leaf extract is used as a reducing, capping agent and fuel for the synthesis of NiO nanoparticles through a green route in the present study. XRD and FT-IR confirms the formation of pure and crystalline NiO nanoparticles, which showed superior performance in cytotoxic activity, antibacterial studies and photocatalytic activity. The cytotoxic activity studies over A549 cell lines were carried out and it showed effective activity. From the antibacterial studies, it is found that NiO activity was more pronounced for Gram positive bacterial strains than Gram negative bacterial strains. The photocatalytic degradation studies confirms its effectiveness towards the complete degradation of 4-CP at pH 8 under the optimized conditions. The mechanism is also proposed wherever required. Thus, we have proposed a green protocol to synthesize an effective biomaterial (NiO nanoparticles) with high purity and crystallinity, reduced particle size, more surface defects and self-assembled morphology, which are the advantageous factors to be used for various environmental and applications.

Acknowledgements

We are thanks to Loyola College management and the authors (R. J. and HAA) also thank the deanship of scientific research, King Saud University, funding through the Vice Deanship of Scientific Research Chair.

References

[1] N. Ajoudanian, A. Nezamzadeh-Ejhieh, Enhanced photocatalytic activity of nickel oxide supported on clinoptilolite nanoparticles for the photodegradation of aqueous cephalexin, Mater. Sci. Semicond. Process. 36 (2015) 162–169.
[2] X. Cai, Y. Cai, Y. Liu, S. Deng, Y. Wang, Y. Wang, I. Djerdj, Photocatalytic degradation properties of Ni (OH) 2 nanosheets/ZnO nanorods composites for azo dyes under visible-light irradiation, Ceram. Int. 40 (2014) 57–65.
[3] S.H. Kim, A. Umar, R. Kumar, A.A. Ibrahim, G. Kumar, Facile synthesis and photocatalytic activity of cocoon-shaped CuO nanostructures, Mater. Lett. 156 (2015) 138–141.
[4] X. Qi, G. Su, G. Bo, L. Cao, W. Liu, Synthesis of NiO and NiO/TiO_2 films with electrochromic and photocatalytic activities, Surf. Coat. Technol. 272 (2015) 79–85.
[5] S. Rakshit, S. Chall, S.S. Mati, A. Roychowdhury, S.P. Moulik, S.C. Bhattacharya, Morphology control of nickel oxalate by soft chemistry and conversion to nickel oxide for application in photocatalysis, RSC Adv. 3 (17) (2013) 6106–6116.

[6] M.A. Fischbach, C.T. Walsh, Antibiotics for emerging pathogens, Science 325 (5944) (2009) 1089–1093.
[7] A.J. Huh, Y.J. Kwon, "Nanoantibiotics": a new paradigm for treating infectious diseases using nanomaterials in the antibiotics resistant era, J. Control. Release 156 (2) (2011) 128–145.
[8] X. Dong, W. Ding, X. Zhang, X. Liang, Mechanism and kinetics model of degradation of synthetic dyes by UV–vis/H_2O_2/ferrioxalate complexes, Dyes Pigments 74 (2) (2007) 470–476.
[9] R. Kumar, C. Baratto, G. Faglia, G. Sberveglieri, E. Bontempi, L. Borgese, Tailoring the textured surface of porous nanostructured NiO thin films for the detection of pollutant gases, Thin Solid Films 583 (2015) 233–238.
[10] S. Berchmans, H. Gomathi, G.P. Rao, Electrooxidation of alcohols and sugars catalysed on a nickel oxide modified glassy carbon electrode, J. Electroanal. Chem. 394 (1-2) (1995) 267–270.
[11] M.H. Huang, Y. Wu, H. Feick, N. Tran, E. Weber, P. Yang, Catalytic growth of zinc oxide nanowires by vapor transport, Adv. Mater. 13 (2) (2001) 113–116.
[12] E.D. Sherly, J.J. Vijaya, L.J. Kennedy, A. Meenakshisundaram, M. Lavanya, A comparative study of the effects of CuO, NiO, ZrO_2 and CeO_2 coupling on the photocatalytic activity and characteristics of ZnO, Korean J. Chem. Eng. 33 (4) (2016) 1431–1440.
[13] S.K. Jesudoss, J.J. Vijaya, L.J. Kennedy, P.I. Rajan, H.A. Al-Lohedan, R.J. Ramalingam, K. Kaviyarasu, M. Bououdina, Studies on the efficient dual performance of $Mn_{1-x}Ni_xFe_2O_4$ spinel nanoparticles in photodegradation and antibacterial activity, J. Photochem. Photobiol. B Biol. 165 (2016) 121–132.
[14] N. Jayaprakash, J.J. Vijaya, L.J. Kennedy, K. Priadharsini, P. Palani, Antibacterial activity of silver nanoparticles synthesized from serine, Mater. Sci. Eng. C 49 (2015) 316–322.
[15] N.M. Basith, J.J. Vijaya, L.J. Kennedy, M. Bououdina, S. Jenefar, V. Kaviyarasan, Co-doped ZnO nanoparticles: structural, morphological, optical, magnetic and antibacterial studies, J. Mater. Sci. Technol. 30 (11) (2014) 1108–1117.
[16] B. Varghese, M.V. Reddy, Z. Yanwu, C.S. Lit, T.C. Hoong, G.V. Subba Rao, B.V. Chowdari, A.T. Wee, C.T. Lim, C.H. Sow, Fabrication of NiO nanowall electrodes for high performance lithium ion battery, Chem. Mater. 20 (10) (2008) 3360–3367.
[17] A.A. Ezhilarasi, J.J. Vijaya, K. Kaviyarasu, M. Maaza, A. Ayeshamariam, L.J. Kennedy, Green synthesis of NiO nanoparticles using Moringa Oleifera extract and their biomedical applications: cytotoxicity effect of nanoparticles against HT-29 cancer cells, J. Photochem. Photobiol. B Biol. 164 (2016) 352–360.
[18] K. Kaviyarasu, C.M. Magdalane, E. Manikandan, M. Jayachandran, R. Ladchumananandasivam, S. Neelamani, M. Maaza, Well-aligned graphene oxide nanosheets decorated with zinc oxide nanocrystals for high performance photocatalytic application, Int. J. Nanosci. 14 (03) (2015) 1550007.
[19] K. Kaviyarasu, A. Ayeshamariam, E. Manikandan, J. Kennedy, R. Ladchumananandasivam, U.U. Gomes, M. Jayachandran, M. Maaza, Solution processing of CuSe quantum dots: photocatalytic activity under RhB for UV and visible-light solar irradiation, Mater. Sci. Eng. B 210 (2016) 1–9.
[20] A. Kar, A.K. Ray, Synthesis of nano-spherical nickel by templating hibiscus flower petals, J. Nanosci. Nanotechnol. 2 (2) (2014) 17–20.
[21] P. Maity, D. Hansda, U. Bandyopadhyay, D.K. Mishra, Biological activities of crude extracts and chemical constituents of bael, *Aegle onal marmelos* (L.) Corr, Indian J. Exp. Biol. 47 (2009) 849.
[22] Suvimol, A. Pranee, Bioactive and volatile compounds of Thai bael fruit (*Aegle marmelous* (L) Corr) as a valuable source of functional food ingredients, Int. Food Res. J. 15 (2008) 45.
[23] L. Badam, S.S. Bedekar, K.B. Sonawane, S.P. Joshi, In vitro antiviral activity of bael (*Aegle marmelos* Corr) upon human coxsackieviruses B1-B6, J. Commun. Disord. 34 (2) (2002) 88–99.
[24] Y.T. Prabhu, K.V. Rao, V.S. Kumar, B.S. Kumari, Synthesis of ZnO nanoparticles by a novel surfactant assisted amine combustion method, Adv. Nanopart. 2 (01) (2013) 45.
[25] G. Sangeetha, S. Rajeshwari, R. Venckatesh, Green synthesis of zinc oxide nanoparticles by aloe barbadensis miller leaf extract: structure and optical properties, Mater. Res. Bull. 46 (12) (2011) 2560–2566.
[26] X.S. Wang, X. Liu, L. Wen, Y. Zhou, Y. Jiang, Z. Li, Comparison of basic dye crystal violet removal from aqueous solution by low-cost biosorbents, Sep. Sci. Technol. 43 (14) (2008) 3712–3731.
[27] X. Liu, X. Wu, H. Cao, R.P. Chang, Growth mechanism and properties of ZnO nanorods synthesized by plasma-enhanced chemical vapor deposition, J. Appl. Phys. 95 (6) (2004) 3141–3147.
[28] H. Zeng, W. Cai, P. Liu, X. Xu, H. Zhou, C. Klingshirn, H. Kalt, ZnO-based hollow nanoparticles by selective etching: elimination and reconstruction of metal—semiconductor interface, improvement of blue emission and photocatalysis, ACS Nano 2 (8) (2008) 1661–1670.
[29] S. Suresh, P. Saravanan, K. Jayamoorthy, S.A. Kumar, S. Karthikeyan, Development of silane grafted ZnO core shell nanoparticles loaded diglycidyl epoxy nanocomposites film for antimicrobial applications, Mater. Sci. Eng. C 64 (2016) 286–292.
[30] Z. Chen, E. Shi, W. Li, Y. Zheng, N. Wu, W. Zhong, Particle size comparison of hydrothermally synthesized cobalt and zinc aluminate spinels, J. Am. Ceram. Soc. 85 (12) (2002) 2949–2955.
[31] X.H. Xia, J.P. Tu, J. Zhang, X.L. Wang, W.K. Zhang, H. Huang, Electrochromic properties of porous NiO thin films prepared by a chemical bath deposition, Sol. Energy Mater. Sol. Cells 92 (6) (2008) 628–633.
[32] Y. Köseoğlu, A. Baykal, M.S. Toprak, F. Gözüak, A.C. Başaran, B. Aktaş, Synthesis and characterization of $ZnFe_2O_4$ magnetic nanoparticles via a PEG-assisted route, J. Alloys Compd. 462 (1) (2008) 209–213.
[33] L. Li, L. Chen, R. Qihe, G. Li, Magnetic crossover of NiO nanocrystals at room temperature, Appl. Phys. Lett. 89 (13) (2006) 134102.
[34] M.K. Roy, M. Kobori, M. Takenaka, K. Nakahara, H. Shinmoto, S. Isobe, T. Tsushida, Antiproliferative effect on human cancer cell lines after treatment with nimbolide extracted from an edible part of the neem tree (*Azadirachta indica*), Phytother. Res. 21 (2007) 243–250.
[35] A.A. Mariam, M. Kashif, S. Arokiyaraj, Bio-synthesis of NiO and Ni nanoparticles and their characterization, Dig. J. Nanomater. Biostruct. 9 (2014) 1007–1019.
[36] M. Horie, K. Nishio, K. Fujita, S. Endoh, A. Miyauchi, Y. Saito, H. Iwahashi, K. Yamamoto, H. Murayama, H. Nakano, N. Nanashima, Protein adsorption of ultrafine metal oxide and its influence on cytotoxicity toward cultured cells, Chem. Res. Toxicol. 22 (3) (2009) 543–553.
[37] M. Lundqvist, J. Stigler, T. Cedervall, T. Berggård, M.B. Flanagan, I. Lynch, G. Elia, K. Dawson, The evolution of the protein corona around nanoparticles: a test study, ACS Nano 5 (9) (2011) 7503–7509.
[38] H. Sun, M. Shamy, M. Costa, Nickel and epigenetic gene silencing, Gene 4 (4) (2013) 583–595.
[39] H. Chen, N.C. Giri, R. Zhang, K. Yamane, Y. Zhang, M. Maroney, M. Costa, Nickel ions inhibit histone demethylase JMJD1A and DNA repair enzyme ABH2 by replacing the ferrous iron in the catalytic centers, J. Biol. Chem. 285 (10) (2010) 7374–7383.
[40] A. Aranda, L. Sequedo, L. Tolosa, G. Quintas, E. Burello, J.V. Castell, L. Gombau, Dichloro-dihydro-fluorescein diacetate (DCFH-DA) assay: a quantitative method for oxidative stress assessment of nanoparticle-treated cells, Toxicol. in Vitro 27 (2) (2013) 954–963.
[41] H. Zhan, T. Suzuki, K. Aizawa, K. Miyagawa, R. Nagai, Ataxia telangiectasia mutated (ATM)-mediated DNA damage response in oxidative stress-induced vascular endothelial cell senescence, J. Biol. Chem. 285 (38) (2010) 29662–29670.
[42] S.M. Helen, H.E. Rani, Characterization and antimicrobial study of nickel nanoparticles synthesized from Dioscorea (elephant yam) by green route, Int. J. Sci. Res. 4 (2015) 216–219.
[43] S. Arokiyaraj, M.V. Arasu, S. Vincent, N.U. Prakash, S.H. Choi, Y.K. Oh, K.C. Choi, K.H. Kim, Rapid green synthesis of silver nanoparticles from *Chrysanthemum indicum* L. and its antibacterial and cytotoxic effects: an in vitro study, Int. J. Nanomedicine 9 (2014) 379.
[44] G. Basak, D. Das, N. Das, Dual role of acidic diacetate sophorolipid as biostabilizer for ZnO nanoparticle synthesis and biofunctionalizing agent against *Salmonella enterica* and *Candida albicans*, J. Microbiol. Biotechnol. 24 (2014) 87–96.
[45] S.K. Jesudoss, J.J. Vijaya, N. Clament, S. Selvam, K. Kombaiah, M. Sivachidambaram, T. Adinaveen, L.J. Kennedy, Effects of Ba doping on structural, morphological, optical, and photocatalytic properties of self-assembled ZnO nanospheres, Clean Technol. Environ. Policy 18 (3) (2016) 729.
[46] P.K. Stoimenov, R.L. Klinger, G.L. Marchin, K.J. Klabunde, Metal oxide nanoparticles as bactericidal agents, Langmuir 18 (17) (2002) 6679–6686.
[47] M. Kokkoris, C.C. Trapalis, S. Kossionides, R. Vlastou, B. Nsouli, R. Grötzschel, S. Spartalis, G. Kordas, T. Paradellis, RBS and HIRBS studies of nanostructured $AgSiO_2$ sol–gel thin coatings, Nucl. Instrum. Methods Phys. Res. 188 (1) (2002) 67–72.
[48] W. Lin, Y.W. Huang, X.D. Zhou, Y. Ma, Toxicity of cerium oxide nanoparticles in human lung cancer cells, Int. J. Toxicol. 25 (6) (2006) 451–457.
[49] S.H. Kim, H.S. Lee, D.S. Ryu, S.J. Choi, D.S. Lee, Antibacterial activity of silver-nanoparticles against *Staphylococcus aureus* and *Escherichia coli*, Kor. J. Microbiol. 39 (1) (2011) 77–85.
[50] M.R. Hoffmann, S.T. Martin, W. Choi, D.W. Bahnemann, Environmental applications of semiconductor photocatalysis, Chem. Rev. 95 (1) (1995) 69–96.
[51] N. Wang, X. Li, Y. Wang, X. Quan, G. Chen, Evaluation of bias potential enhanced photocatalytic degradation of 4-chlorophenol with TiO_2 nanotube fabricated by anodic oxidation method, Chem. Eng. J. 146 (1) (2009) 30–35.
[52] U.I. Gaya, A.H. Abdullah, Z. Zainal, M.Z. Hussein, Photocatalytic treatment of 4-chlorophenol in aqueous ZnO suspensions: intermediates, influence of dosage and inorganic anions, J. Hazard. Mater. 168 (1) (2009) 57–63.
[53] M. Stoyanova, S. Christoskova, Catalytic degradation of methylene blue in aqueous solutions over Ni- and Co-oxide systems, Cent. Eur. J. Chem. 9 (6) (2011) 1000–1007.
[54] S. Sakthivel, M.V. Shankar, M. Palanichamy, B. Arabindoo, D.W. Bahnemann, V. Murugesan, Enhancement of photocatalytic activity by metal deposition: characterisation and photonic efficiency of Pt, Au and Pd deposited on TiO_2 catalyst, Water Res. 38 (13) (2004) 3001–3008.
[55] N.C. Selvam, S. Narayanan, L.J. Kennedy, J.J. Vijaya, Pure and Mg-doped self-assembled ZnO nano-particles for the enhanced photocatalytic degradation of 4-chlorophenol, J. Environ. Sci. 25 (10) (2013) 2157–2167.
[56] C.H. Chiou, C.Y. Wu, R.S. Juang, Influence of operating parameters on photocatalytic degradation of phenol in UV/TiO_2 process, Chem. Eng. J. 139 (2) (2008) 322–329.
[57] E. Agulló, E. Expósito, V. Montiel, A. Aldaz, Influence of an ultrasonic field on lead electrodeposition on copper using a fluoroboric bath, New J. Chem. 23 (1) (1999) 95–101.
[58] R. Chauhan, A. Kumar, R.P. Chaudhary, Structural and photocatalytic studies of Mn doped TiO_2 nanoparticles, Spectrochim. Acta A Mol. Biomol. Spectrosc. 98 (2012) 256–264.
[59] K. Kaviyarasu, C. Maria Magdalane, K. Kanimozhi, J. Kennedy, B. Siddhardha, E. Subba Reddy, R. Naresh Kumar, S. Chandra Shekhar, F.T. Thema, D. Letsholathebe, G.T. Mola, M. Maaza, Elucidation of photocatalysis, photoluminescence and antibacterial studies of ZnO thin films by spin coating method, J. Photochem. Photobiol. B Biol. 173 (2017) 466–475.
[60] C. Maria Magdalane, K. Kaviayarasu, J. Judith Vijaya, C. Jayakumar, M. Maaza,

B. Jeyaraj, Photocatalytic degradation effect of malachite green and catalytic hydrogenation by UV–illuminated CeO_2/CdO multilayered nanoplatelet arrays: investigation of antifungal and antimicrobial activities, J. Photochem. Photobiol. B Biol. 169 (2017) 110–123.

[61] K. Kaviyarasu, L. Kotsedi, A. Simo, X. Fuku, G.T. Mola, J. Kennedy, M. Maaza, Photocatalytic activity of ZrO_2 doped lead dioxide nanocomposites: investigation of structural and optical microscopy of RhB organic dye, Appl. Surf. Sci. 421 (2017) 234–239.

[62] C. Maria Magdalane, K. Kaviayarasu, J. Judith Vijaya, B. Siddhardha, B. Jeyaraj, Facile synthesis of heterostructured cerium oxide/yttrium oxide nanocomposite in UV light induced photocatalytic degradation and catalytic reduction: synergistic effect of antimicrobial studies, J. Photochem. Photobiol. B Biol. 173 (2017) 23–34.

[63] X. Fuku, N. Matinise, M. Masikini, K. Kaviyarasu, M. Maaza, An electrochemically active green synthesized polycrystalline NiO/MgO catalyst: use in photo-catalytic applications, Mater. Res. Bull. 97 (2018) 457–465.

[64] K. Kaviyarasu, A. Mariappan, K. Neyvasagam, A. Ayeshamariam, P. Pandi, R.P. Palanichamy, C. Gopinathan, G.T. Mola, M. Maaza, Photocatalytic performance and antimicrobial activities of HAp-TiO_2 nanocomposite thin films by sol–gel method, Surf. Interface Anal. 6 (2017) 247–255.

[65] P. Iyyappa Rajan, J. Judith Vijaya, S.K. Jesudoss, K. Kaviyarasu, L. John Kennedy, R. Jothiramalingam, Hamad A. Al-Lohedan, Mansoor-Ali Vaali-Mohammed, Green-fuel-mediated synthesis of self-assembled NiO nano-sticks for dual applications-photocatalytic activity on Rose Bengal dye and antimicrobial action on bacterial strains, Mater. Res. Exp. 4 (8) (2017) 085030.

[66] C. Maria Magdalane, K. Kaviayarasu, J. Judith Vijaya, B. Siddhardha, B. Jeyaraj, J. Kennedy, M. Maaza, Evaluation on the heterostructured CeO_2/Y_2O_3 binary metal oxide nanocomposites for UV/Vis light induced photocatalytic degradation of Rhodamine-B dye for textile engineering application, J. Alloys Compd. 727 (2017) 1324–1337.

[67] J. Judith Vijaya, N. Jayaprakash, K. Kombaiah, K. Kaviayarasu, L. John Kennedy, R. Jothiramalingam, Hamad A. Al-Lohedan, Mansoor-Ali Vaali-Mohammed, M. Maaza, Bioreduction potentials of dried root of *Zingiber officinale* for a simple green synthesis of silver nanoparticles: antibacterial studies, J. Photochem. Photobiol. B Biol. 177 (2017) 62–68.

[68] M. Siva Chidambaram, J. Judith Vijaya, K. Kaviyarasu, L. John Kennedy, R. Jothiramalingam, Hamad A. Al-Lohedan, A novel synthesis protocol for Co_3O_4 nanocatalysts and their catalytic applications, RSC Adv. 7 (2017) 38861–38870.

[69] N. Jayaprakash, J. Judith Vijaya, K. Kaviayarasu, K. Kombaiah, L. John Kennedy, R. Jothiramalingam, Murugan A. Munusamy, Hamad A. Al-Lohedan, Green synthesis of Ag nanoparticles using tamarind fruit extract for the antibacterial studies, J. Photochem. Photobiol. B Biol. 169 (2017) 178–185.

[70] K. Kaviyarasu, J. Kennedy, E. Manikandan, M. Henini, M. Maaza, Photodegradation of organic pollutants RhB dye using UV simulated sunlight on ceria based TiO_2 nanomaterials for antibacterial applications, Sci. Rep. 6 (2016) 38064.

[71] K. Kaviyarasu, K. Kanimozhi, N. Matinise, C. Maria magdalane, G.T. Mola, J. Kennedy, M. Maaza, Antiproliferative effects on human lung cell lines A549 activity of cadmium selenide nanoparticles extracted from cytotoxic effects: investigation of bio-electronic application, Mater. Sci. Eng. C 76 (2017) 1012–1025.